The Role of Ocean Dynamical Thermostat in Delaying the El Niño–Like Response over the Equatorial Pacific to Climate Warming

YIYONG LUO

Physical Oceanography Laboratory/CIMST, Ocean University of China, and Qingdao National Laboratory for Marine Science and Technology, Qingdao, China

JIAN LU

Atmospheric Sciences and Global Change Division, Pacific Northwest National Laboratory, Richland, Washington

FUKAI LIU

Physical Oceanography Laboratory/CIMST, Ocean University of China, and Qingdao National Laboratory for Marine Science and Technology, Qingdao, China

OLUWAYEMI GARUBA

Atmospheric Sciences and Global Change Division, Pacific Northwest National Laboratory, Richland, Washington

(Manuscript received 15 June 2016, in final form 11 September 2016)

ABSTRACT

The role of ocean dynamics in the response of the equatorial Pacific Ocean to climate warming is investigated using both an atmosphere–ocean coupled climate system and its ocean component. Results show that the initial response (fast pattern) to an uniform heating imposed on the ocean is a warming centered to the west of the date line owing to the conventional ocean dynamical thermostat (ODT) mechanism in the eastern equatorial Pacific—a cooling effect arising from the up-gradient upwelling. In time, the warming pattern gradually propagates eastward, becoming more El Niño–like (slow pattern). The transition from the fast to the slow pattern likely results from 1) the gradual warming of the equatorial thermocline temperature, which is associated with the arrival of the relatively warmer extratropical waters advected along the subsurface branch of the subtropical cells (STCs), and 2) the reduction of the STC strength itself. A mixed layer heat budget analysis finds that it is the total ocean dynamical effect rather than the conventional ODT that holds the key for understanding the pattern of the SST in the equatorial Pacific and that the surface heat flux works mainly to compensate the ocean dynamics. Further passive tracer experiments with the ocean component of the coupled system verify the role of the ocean dynamical processes in initiating a La Niña–like SST warming and in setting the pace of the transition to an El Niño–like warming and identify an oceanic origin for the slow eastern Pacific warming independent of the weakening trade wind.

1. Introduction

It has long been recognized that ocean dynamics plays an important role in the regulation of the equatorial Pacific sea surface temperature (SST). Through a suite of experiments with a simplified coupled atmosphere–ocean model forced by a uniform heating into the ocean surface, Clement et al. (1996) first identified a so-called ocean dynamical thermostat (ODT) mechanism, which refers to the damping effect on the SST warming through the divergence of the heat by the oceanic upwelling in the central and eastern equatorial Pacific upon an imposed surface heating, while in the western tropical Pacific the SST must warm as much as necessary for the upward surface heat flux to balance the imposed downward flux since the ocean heat advection is relatively feeble there. Consequently, the equatorial SST warms less in the east than in the west. This means that the east–west SST gradient is increased and the

Denotes Open Access content.

Corresponding author e-mail: Yiyong Luo, yiyongluo@ouc.edu.cn

DOI: 10.1175/JCLI-D-16-0454.1

equatorial easterlies are thus strengthened, which in turn enhances the upwelling and causes the thermocline to shoal in the eastern Pacific. Both ocean dynamical processes cool the SST in the eastern Pacific and strengthen the equatorial SST gradient, leading to a La Niña–like pattern over the equatorial Pacific. This conventional ODT has been adopted to account for the distinct Pacific SST patterns in response to global warming between a climate system with an atmosphere coupled to a slab ocean versus the fully coupled climate system with ocean dynamics (Vecchi et al. 2008).

The main shortcoming in Clement et al.'s model is that the temperature of the thermocline water that is upwelled does not respond to the variations in SST (i.e., the thermocline temperature adjustment is not allowed in their model). To address this weakness, Seager and Murtugudde (1997) employed an ocean general circulation model (GCM) thermodynamically coupled to an advective atmospheric mixed layer model (Seager et al. 1995) with the atmospheric variables such as winds, solar radiation, and clouds externally prescribed. Therefore the thermal coupling is better represented than the dynamical coupling in their model. They found that, in the absence of the wind stress feedback, the inclusion of thermocline temperature adjustment still gives way to the ODT mechanism, resulting in an SST minimum in the eastern equatorial Pacific under a uniform surface heat flux forcing to the ocean. This result is in direct contrast with the coupled atmosphere–ocean GCM simulation of Knutson and Manabe (1995), who demonstrated that increasing greenhouse gases (GHGs) induce a reduction of the zonal SST gradient due to stronger evaporative cooling over the warm pool than the cold tongue. Seager and Murtugudde (1997) suggested that this contradiction is possibly the result of the low resolution in Knutson and Manabe's model. However, this attribution may be ruled out by recent studies, in which a majority of climate models with the latest improvements in parameterizations and resolution tends to project an El Niño–like response in the equatorial Pacific to increasing GHGs (e.g., Jia and Wu 2013; Luo et al. 2015; Li et al. 2016; Liu et al. 2016). Taken together, one might surmise that the weaker Walker cell mechanism proposed by Vecchi et al. (2008) might be the ultimate source for the El Niño–like response via Bjerknes feedback. However, through careful diagnosis of the air–sea energy budget and ocean heat transport, DiNezio et al. (2009, 2010) dismissed El Niño as a useful analogy for the equatorial Pacific warming under increasing GHGs by noting that the impact of ocean dynamical response is to damp the warm signal over the eastern equatorial Pacific. Thus, jury is still out regarding the real source for the El Niño–like warming simulated by the latest climate models.

Other studies found that the response of the equatorial Pacific Ocean to abrupt CO_2 forcing experiences a fast phase and a slow phase. In particular, Held et al. (2010) investigated the fast and slow components of global warming using the Geophysical Fluid Dynamics Laboratory (GFDL) climate model, and found that in the tropics the fast pattern is featured with maximum warming in the west, but this warming moves to the east Pacific, becoming more El Niño–like over time. Andrews et al. (2015) analyzed phase 5 of the Coupled Model Intercomparison Project (CMIP5) models and found that in the tropical Pacific the warming is delayed in the east after an abrupt quadrupling of CO_2 levels, while on multidecadal time scales the eastern tropical Pacific warms significantly more than the west and the tropical warming pattern becomes more El Niño–like. However, how this response pattern transitions to be El Niño–like in the slow phase remains unexplained in those studies.

Here, in the spirit of Clement et al. (1996) and Seager and Murtugudde (1997), we impose a uniform energy flux into the ocean in the Community Earth System Model version 1.1 (CESM1.1) of the National Center for Atmospheric Research (NCAR). As will be shown later, we also find transitions similar to those of Held et al. (2010) and Andrews et al. (2015) from a west-heavy SST warming to an El Niño–like, east-heavy SST warming with time. This experiment design will be referred to as ''ODT-type'' experiments in the context of this study. The fact that our ODT experiment with CESM1.1 can reproduce the fast-to-slow SST pattern transition hints that the details in the structure of the heating for the ocean and the associated atmospheric thermal and radiative feedbacks are not the root cause for the large-scale evolution of the Pacific SST. Further, we design a passive tracer and deploy it to an ODT experiment using only the ocean component of the CESM1.1 to demonstrate unambiguously an oceanic origin of the initial La Niña–like response and reveal a possible additional oceanic origin of the weakening of the Pacific subtropical overturning cell (STC), the process underpinning the slow transition to the El Niño–like state. Together with the coupled ODT experiment, our tracer experiments help shed new light on the ultimate source for the El Niño–like SST response to global warming. Moreover, the findings in this study also expand the physical meaning of the ODT and perpetuate its importance in shaping the global SST response under a changing climate.

TABLE 1. Experiment sets with CESM1.1 and its ocean component POP2.

Name	Run (yr)	Description
		Coupled ODT experiments (CESM1.1)
CTRL	100	Control run initiated from the long equilibrated state
HEAT	9×100	Adding uniform 6 W m^{-2} to the ocean (nine members)
		SST and tracer restoring experiments (POP2)
Picontrol	50	Restoring surface fluxes toward an equilibrated climatology from CCSM4 piControl experiment
Perturbation	50	Same as above, but the restoration SST is perturbed by 3.2 K
P_1' tracer	50	A passive tracer is added to the perturbation run and restored to the 3.2 K surface anomaly
P_2' tracer	50	A passive tracer is added to the picontrol run and restored to the 3.2-K surface anomaly

The rest of the paper is structured as follows. Section 2 describes the experiment design for both CESM1.1 coupled experiments and the ocean-alone tracer experiments. Section 3 presents the fast and slow response patterns. A mixed layer heat budget analysis is conducted in section 4 to understand the formation mechanisms of these patterns in the coupled ODT experiments. Section 5 investigates the mechanisms of the transition from a pattern with more warming in the west to an El Niño–like pattern, leveraging on the ocean-alone tracer experiments. Section 6 summarizes our main findings in this study and discusses the possible open issues.

2. Models and experiments

a. *Experiments with CESM1.1*

The model CESM1.1 comprises the Community Atmospheric Model version 5 (CAM5), the Community Land Model version 4 (CLM4), and the Parallel Ocean Program version 2 (POP2). The horizontal resolution of CAM5 and CLM4 is 1.9° longitude × 1.9° latitude, with the atmospheric component having 30 vertical levels. The horizontal resolution of the POP2 is nominal 1°, telescoped meridionally to ~0.3° at the equator. Vertically, it has 60 uneven levels with the thickness varying from 10 m near the surface to 250 m at the bottom.

Starting from an equilibrium state that is available at NCAR, a control simulation (CTRL) is first integrated for 100 years with no external forcing in the coupled atmosphere–ocean system. An ensemble of nine heating simulations (HEAT) is then performed by adding a uniform heat flux of 6 W m^{-2} into the ocean surface with each of the ensemble member differing only in the initial condition (Table 1). The response presented below is taken as the difference between HEAT and CTRL (HEAT minus CTRL). Under the uniform heat flux prescribed as such, the air–sea coupling at the surface works to offset it by releasing more heat into the atmosphere. As shown in Fig. 1a, both the net flux into the ocean and the heat release from the ocean to the atmosphere take an *e*-folding path toward their respective final equilibrium values: 0 W m^{-2} for the former and 6 W m^{-2} for the later. However, because of the large heat capacity and the slow time scale for the deep ocean to reach new equilibrium, the net heat flux to the ocean remains larger than 1 W m^{-2} by the end of the integration at year 100 (Fig. 1a). Indeed, by then most of heat goes to the deep ocean, as one can infer from the rate of the increase of the deep ocean heat content (Fig. 1b). In the sense that the coupled ODT simulation would eventually asymptote to new equilibrium, it resembles the coupled model simulation under an abrupt increase of CO_2 concentration, both requiring thousands of years of model integration to finally reach equilibrium (Li et al. 2013).

Figure 2 shows global-mean SST from nine members of the CESM1.1 simulations in response to the uniform heating into the ocean surface. The SST warms rapidly during the first 10 years, and then the pace of the warming slows down with time. Thus, it is clear that while the system is still adjusting toward the equilibrium, the upper ocean can be thought of as reaching a quasi-equilibrium stage after ~80 years of the model integration. The fast and slow time scales of response are in agreement with previous climate model simulations (e.g., Held et al. 2010; Knutti et al. 2008). For example, Held et al. (2010) found that the surface temperature response to doubling CO_2 consists of a fast component (an exponential evolution of SST over the first 3–5 years) and a slow component (the warming evolves more slowly after 20 years). In addition, a simple two-box model has been used to provide a physical interpretation of the fast and slow response (e.g., Gregory 2000; Held et al. 2010; Long et al. 2014). In this work, the first decade (from year 1 to year 10) is taken as the fast response phase, and the last two decades (from year 81 to year 100) as the slow response phase.

b. *Passive tracer experiments with POP2*

Passive tracer experiments have been widely employed to illustrate the effect of the ocean circulation and mixing and the change thereof on the ocean heat uptake under climate change (e.g., Banks and Gregory

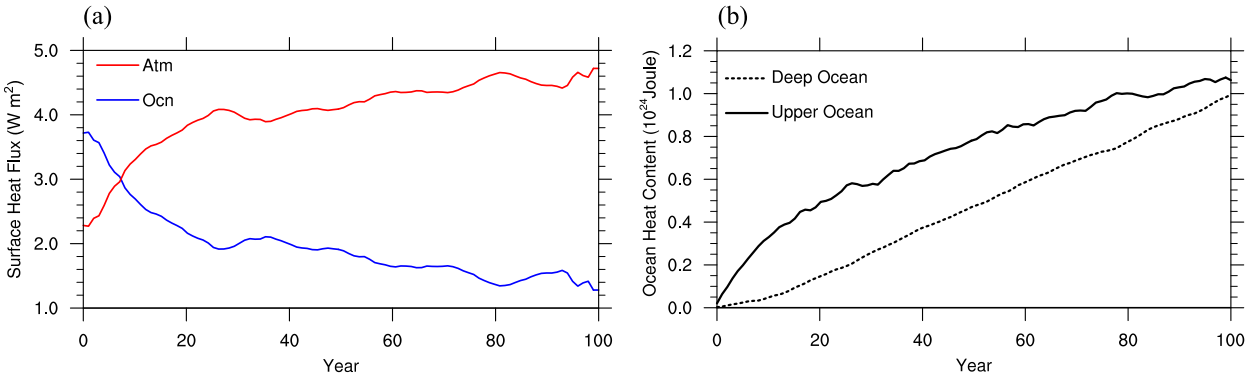

FIG. 1. Ensemble mean time series of (a) the heat released to the atmosphere (red) and the heat entering the ocean (blue) at the air–sea interface, and (b) ocean heat content of upper ocean (0–500 m; solid) and deep ocean (500–6000 m; dashed) in the nine-member coupled experiments with CESM1.1.

2006; Xie and Vallis 2012). To further diagnose the origin of the initial minimum warming and the emergence of the El Niño–like warming in the eastern equatorial Pacific, we employ a passive tracer with the POP2 ocean model in order to isolate the contribution to the SST change due to the passive advection and mixing by the background mean circulation from that due to the change of ocean circulation. For the ocean temperature governed by the advection–diffusion processes, the governing equation can be written as

$$\frac{\partial T}{\partial t} = Q - \nabla \cdot (\mathbf{v}T), \tag{1}$$

in which the advection is carried out by the generalized velocity $\mathbf{v}(x, y, z, t)$ including a bolus component parameterizing eddy and subgrid turbulence effects. The term Q is the net surface heat flux into the ocean. For a perturbed ocean by a surface flux anomaly Q', the evolution of the ocean temperature anomalies is governed by

$$\frac{\partial T'}{\partial t} = Q' - \nabla \cdot (\mathbf{v}'\overline{T}) - \nabla \cdot (\overline{\mathbf{v}}T'). \tag{2}$$

The perturbation heat flux is configured as a linear relaxation of the SST toward a uniform target temperature $T'_\star$ with a relaxation time scale $1/\alpha$, that is, $Q' = \alpha(T'_\star - T'_S)$, where subscript S indicates the surface value.

To isolate the passive advective effect on the ocean heat uptake, in the spirit of Banks and Gregory (2006), we introduce the passive tracer P' and initialize it at zero but force it with a restoration $Q'_p = \alpha(T'_\star - P'_S)$. The evolution of P' is governed by

$$\frac{\partial P'}{\partial t} = Q'_p - \nabla \cdot (\overline{\mathbf{v}}P'). \tag{3}$$

Note that although both T' and P' are restored toward the same target temperature anomaly, the resultant fluxes differ by $-\alpha(T'_\star - P'_S)$, a surface flux difference induced by the reservoir redistribution of the ocean temperature [see Garuba and Klinger (2016) for detailed explanation]. By estimating P' as such, the total evolution of T' can be decomposed into a passively advective component P' and an inferred redistributive component T'_r through $T' = T'_r + P'$. Subtracting (3) from (2) yields the equation for T'_r:

$$\frac{\partial T'_r}{\partial t} = (Q' - Q'_p) - \nabla \cdot (\mathbf{v}'\overline{T}) - \nabla \cdot (\overline{\mathbf{v}}T'_r). \tag{4}$$

Unlike the conventional redistributive temperature, the global volume integral of T'_r is not zero; this is because of the nonzero surface flux $(Q' - Q'_p)$ induced by T'_r itself.

By construction, the temperature anomalies T' can always be decomposed as such regardless of the spatial structure of Q'. To highlight the role of

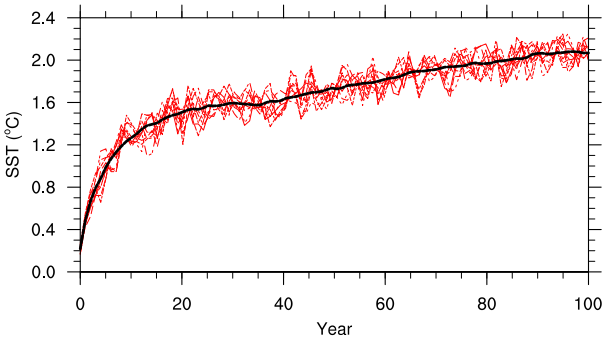

FIG. 2. Time evolution of global-mean SST from the nine-member coupled experiments using CESM1.1, with each individual member represented by a thin red line and the ensemble mean by the thick black line.

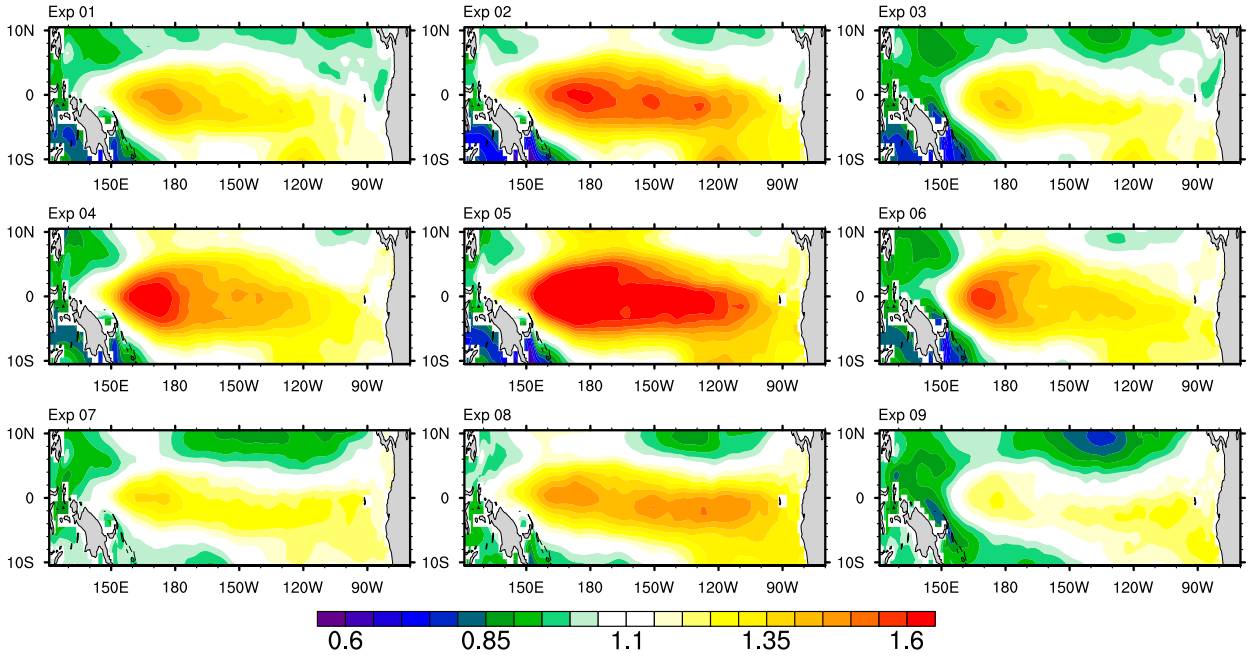

FIG. 3. The fast response patterns of SST (°C) from nine heating simulations with CESM1.1.

oceanic processes in the SST pattern formation, we restore the SST anomalies and passive tracer anomalies toward a uniform 3.2 K [i.e., the average of the global SST warming during years 100–150 in the abrupt $4\times CO_2$ experiment using Community Climate System Model version 4 (CCSM4)] in the SST perturbation experiment and the passive tracer experiment, respectively. Importantly, because both the target temperature $T'_\star$ and the restoring coefficient α are uniform in space, and all other air–sea fluxes are held fixed at their control value, any spatial structure in the response can only be attributed to oceanic processes. The passive tracer P' helps further isolate the effect of the passive advection and diffusion by the mean background ocean circulation. Together with the coupled ODT experiments above, this decomposition through tracer simulation assists to reveal the ocean dynamical origin for the initial La Niña–like pattern and its transition toward a more El Niño–like state with time.

Specifically, the experiment set consists of the following four runs (Table 1):

- *Picontrol run*: This is forced by restoring the surface conditions toward the climatology derived from the CCSM4 CMIP5 piControl experiment averaged over the nearly equilibrated last 100 years.
- *Perturbation run*: This uses the same surface conditions as the picontrol run except a uniform restoration temperature anomaly (3.2 K) is added to the target temperature.
- P'_1 *Tracer run*: Here a passive tracer is added in the perturbation run and restored to the 3.2-K surface temperature anomaly.
- P'_2 *Tracer run*: a passive tracer is added in the picontrol run and restored to the 3.2-K surface temperature anomaly.

The difference between the picontrol and perturbation runs (i.e., T') gives the warming response governed by the full temperature [(2)]. The passive tracer P'_2 reflects the effect of the passive advection of the heat uptake from the surface by the control current. The difference $P'_1 - P'_2$ reveals the subtle difference between the passive advections by the difference in the ocean currents between the perturbation and picontrol runs.

3. Fast and slow response patterns

Figure 3 shows the fast response patterns of SST from each of the nine heating simulations, and their ensemble mean is shown in Fig. 4a. In eight of the nine simulations, the SST response over the equatorial Pacific is characteristic of a stronger warming in the west than in the east (i.e., an increased zonal gradient of SST along the equator). In contrast, it becomes El Niño–like in the slow response pattern (Fig. 4b), with the maximum warming moving to the central and eastern Pacific.

Figure 4 compares the ensemble mean fast and slow response patterns in SST and wind stress (Figs. 4a,b),

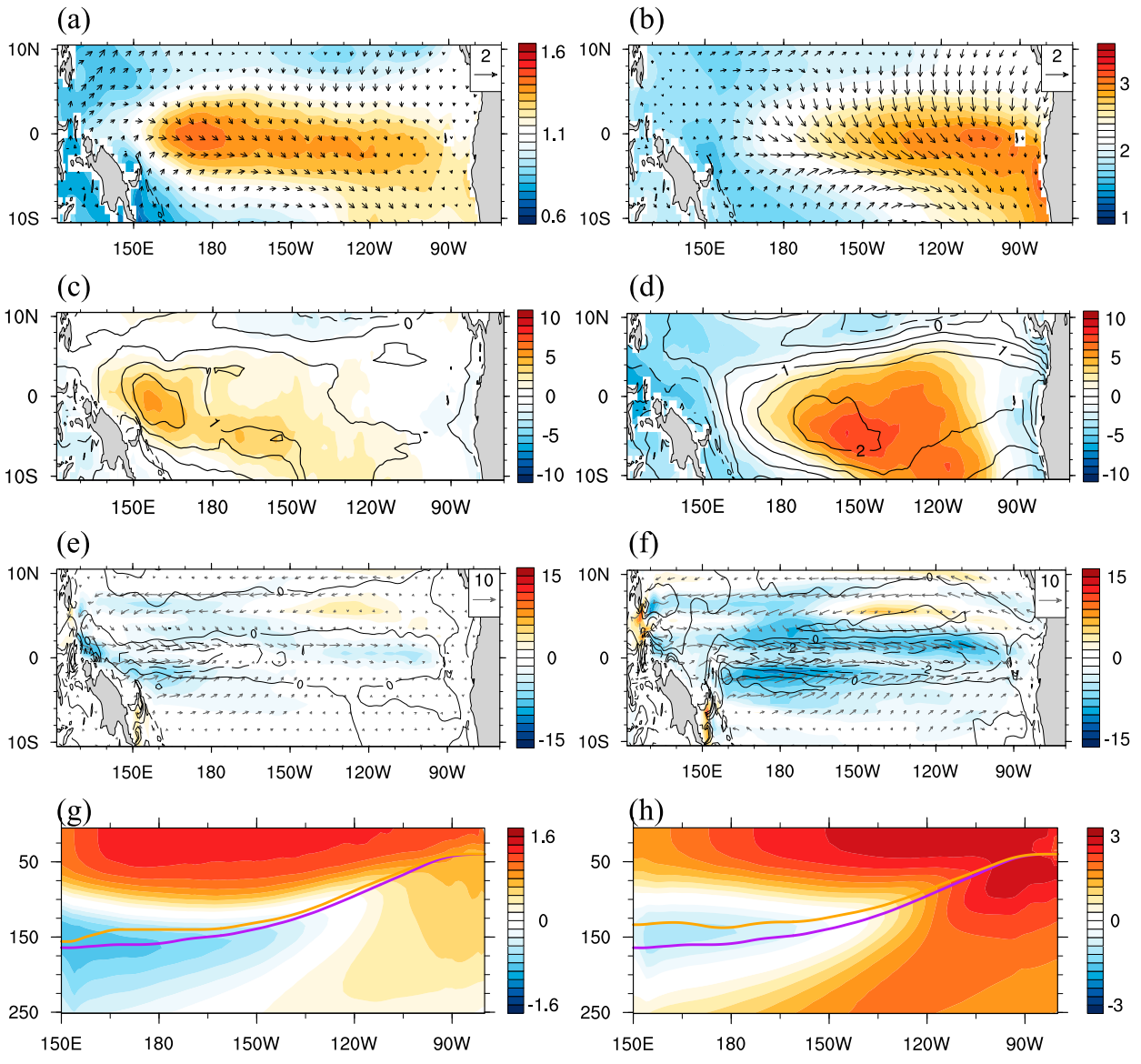

FIG. 4. The (left) fast and (right) slow response patterns: (a),(b) SST (color; °C) and wind stress (vectors; 10^{-2} Pa), (c),(d) total cloud (color; %) and precipitation (contour interval = 0.5 mm day^{-1}), (e),(f) horizontal velocity averaged over the top 50 m [vectors; cm s^{-1} with red (blue) color representing its strengthening (weakening)] and vertical velocity at depth of 50 m (contour interval = 1×10^{-4} cm s^{-1}), and (g),(h) temperature (color; °C) and thermocline depths (thick purple line for CTRL and thick orange line for HEAT) at the equator. Presented here and in Figs. 5–7 are ensemble means from nine heating simulations with CESM1.1.

total cloud amount and precipitation (Figs. 4c,d), horizontal velocity averaged over the top 50 m and vertical velocity at depth of 50 m (Figs. 4e,f), and temperature and thermocline depths at the equator (Figs. 4g,h). In the fast response, over the western equator there appears a weak weakening of the easterlies ($\sim 0.5 \times 10^{-2}$ Pa), an increase of both cloud ($\sim$4%) and precipitation ($\sim$1.5 mm day^{-1}), and a reduction of both the South Equatorial Current (SEC; $\sim$5 cm s^{-1}) and upwelling ($\sim 1 \times 10^{-4}$ cm s^{-1}). In the slow response, changes in these variables become more significant and move to the central and eastern equator, where the weakening of the easterly stress reaches $\sim 1.5 \times 10^{-2}$ Pa, the increase of the cloud and precipitation is $\sim$6% and $\sim$2.0 mm day^{-1}, and the reduction of the SEC and upwelling is $\sim$7 cm s^{-1} and $\sim 2 \times 10^{-4}$ cm s^{-1}, respectively. Accompanying these changes at the sea surface is a change in the upper ocean thermocline structure. While the maximum warming is located at the western equatorial Pacific and spreads to a depth of $\sim$50 m in the fast pattern, it moves to the central and eastern equator and penetrates cross the thermocline into the subsurface

ocean as deep as 150 m in the slow pattern. However, in both the fast and slow patterns, there appears a cooling and an accompanied shoaling of the thermocline over the western and central subsurface equatorial ocean. These above changes during the slow response are similar to what happens in the fully coupled model with the increase of GHG in the atmosphere beginning to level off (e.g., Jia and Wu 2013; Luo et al. 2015; Li et al. 2016; Liu et al. 2016).

4. Mixed layer heat budget analysis

In this section, we examine the mixed layer heat budget to elucidate the processes that maintain the warming patterns during both the fast and slow response. Two regions are selected to represent the different characteristics of the slow and fast response of SST: the western equatorial Pacific (WEP; 5°S–5°N, 135°E–180°) and the central and eastern equatorial Pacific (CEP; 5°S–5°N, 160°–105°W). Following Luo et al. (2015) and Liu et al. (2016), the heat budget analysis is performed with constant depth of 50 m to diagnose the maintaining terms (net surface heat flux; zonal, meridional, and vertical advection; and diffusion) for the SST changes simulated by the experiments. The net surface heat flux is obtained by subtracting the heat penetration at the water depth of 50 m from the surface heat flux. Note that the diffusion here represents the ocean heat transport by all subgrid processes, and a positive (negative) value indicates a heating (cooling).

Figure 5 shows the changes in SST, zonal advection, meridional advection, vertical advection, diffusion, and net surface heat flux for the fast and slow response. In the fast pattern (Fig. 5a), over the WEP, the meridional advection is the major warming source, which is mainly balanced by the cooling from both the diffusion and net surface heat flux, whereas over the CEP both the zonal and meridional advection act to warm the surface ocean, and the diffusion and vertical advection contribute as a cooling effect—the signature of the conventional ODT. In the slow pattern (Fig. 5b), there are warming anomalies of the zonal and meridional advection and cooling anomalies of the vertical advection and net surface heat flux over both WEP and CEP, while the diffusion exerts a cooling effect in the west but a warming effect in the east. Note that, although the conventional ODT is still operating over the CEP region in the slow response phase, the horizontal advective and diffusive warming there overpowers the vertical advective cooling, leading to a net warming. Therefore, the total ocean dynamical effect is opposite to the conventional ODT in the CEP, with the former playing a warming role but the latter a cooling role.

Our modeling results suggest that the total ocean dynamical effect plays a decisive role for the equatorial Pacific SST pattern, while the net surface heat flux works just to compensate the ocean dynamics. In the fast response phase (Fig. 5a), for example, the maximum (minimum) warming in the west (east) corresponds to the warming (cooling) effect from the ocean dynamics, while the net surface heat flux is cooling (warming) in the west (east). Thus, the sign of the SST gradient is dictated by the sign of the total ocean dynamical effect. In the slow response (Fig. 5b), the net surface heat flux cools more in the east than the west, despite more warming in the east than the west. This again suggests the dominant role of the ocean dynamics, while the net surface heat flux acts to counterbalance the ocean dynamical processes so as to ensure a small heat content tendency in the budget. In addition, the sign of SST gradient follows that of the net ocean dynamical effect, which itself results from the competition between the horizontal advection and the vertical advection, with the former dominating the latter. This analysis reveals that the conventional ODT of Clement et al. (1996) is still working against the warming in the CEP even in the slow development of the El Niño–like warming. All in all, it appears that the ocean dynamics holds the key for understanding the pattern of the SST in the equatorial Pacific, and the surface thermal coupling may be just the feedback to the ocean dynamics. This posits a different view in regard to the origin of the El Niño–like warming from previously believed, namely that the air–sea thermal coupling and cloud radiative feedback are the key for the El Niño–like warming in the equatorial Pacific (e.g., Knutson and Manabe 1995; Meehl and Washington 1996; Li et al. 2016). Our further passive tracer experiments with POP2 (even in the absence of wind forcing) indeed point to an oceanic origin for the El Niño–like warming (see section 5b).

To further delineate the cooling effect by the conventional ODT, we decompose the change in the vertical advection term between HEAT and CTRL as follows:

$$\begin{aligned}(W\times S)_{\mathrm{HEAT}} - (W\times S)_{\mathrm{CTRL}} &= (W_{\mathrm{CTRL}} + W')\times(S_{\mathrm{CTRL}} + S') - W_{\mathrm{CTRL}}\times S_{\mathrm{CTRL}} \\ &= W_{\mathrm{CTRL}}\times S' + W'\times S_{\mathrm{CTRL}} + W'\times S', \end{aligned} \tag{5}$$

where the vertical advection is expressed as the product of upwelling W and stratification S at the bottom of the mixed layer, respectively; the primes denote differences

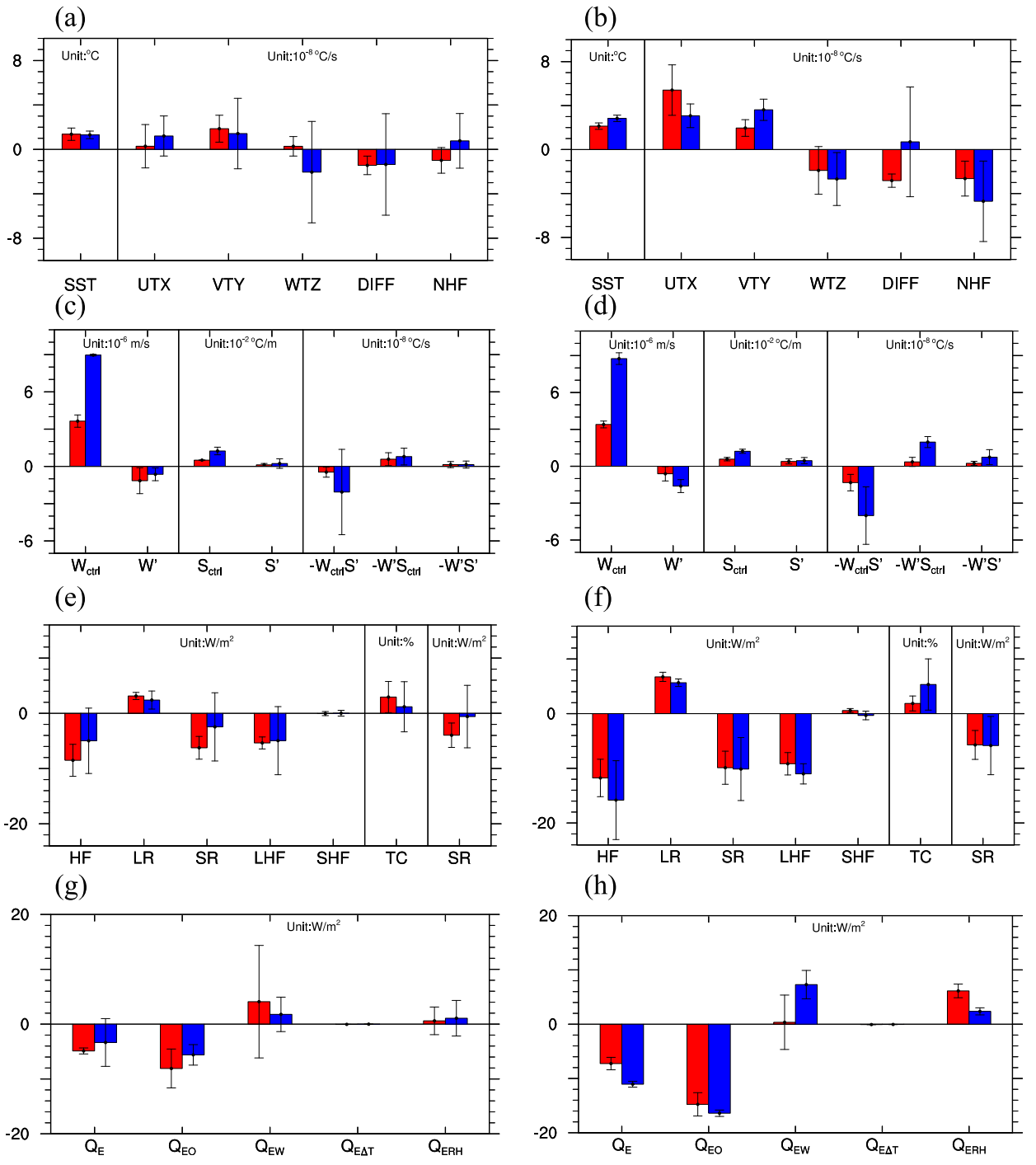

FIG. 5. Changes in the mixed layer heat budget for the (left) fast and (right) slow response patterns: (a),(b) temperature (SST), zonal advection (UTX), meridional advection (VTY), vertical advection (WTZ), diffusion (DIFF), and net surface heat flux (NHF); (c),(d) upwelling (W_{CTRL}) and stratification (S_{CTRL}) at a depth of 50 m derived from the control run and their changes (W' and S') as well as a decomposition of WTZ changes ($W_{\mathrm{CTRL}} \times S'$, $W' \times S_{\mathrm{CTRL}}$, and $W' \times S'$); (e),(f) a decomposition of surface heat flux (HF) changes into longwave radiation (LR), shortwave radiation (SR), latent heat flux (LHF), and sensible heat flux (SHF); and (g),(h) a further decomposition of LHF changes (Q_E) into Newtonian cooling (Q_{EO}), and contributions from atmospheric forcing changes in wind speed (Q_{EW}), relative humidity (Q_{ERH}), and air–sea surface temperature difference ($Q_{E\Delta T}$). In (e) and (f), TC and SR represent the total cloud amount and net downward shortwave radiation at the top of the atmosphere, respectively. Red bars represent the WEP region and blue bars represent the CEP region. The error bars indicate two-standard deviation spreads in the nine-member CESM1.1 ensemble.

between HEAT and CTRL. It is clear that, in both the fast pattern (Fig. 5c) and slow pattern (Fig. 5d), an increase of the stratification induces a cooling ($W_{\mathrm{CTRL}} \times S'$) and a weakening of the upwelling results in a warming ($W' \times S_{\mathrm{CTRL}}$ and $W' \times S'$). In the CEP, the former appears to be significantly greater than the latter, leading to the net cooling effect by the ODT. Therefore, it is the intensified stratification under the uniform heating that is behind the cooling effect of the ODT in the CEP, while the response of the upwelling actually contributes to warm the surface water across the entire equator. In the WEP, there appears to have a significant change in the vertical advection, that is, from a warming effect in the fast phase to a cooling effect in the slow phase (cf. Figs. 5a and 5b). This is again a result of the change of the stratification there; the cooling due to the increased stratification exceeds the warming due to the weakened upwelling in the latter phase (Fig. 5d).

Another significant change in the heat budget balance is the net surface heat flux over the CEP, which is a warming effect for the fast pattern but turns into a cooling effect for the slow pattern (cf. Figs 5a and 5b). To understand this change, we decompose the surface heat flux into four components: longwave radiation, shortwave radiation, latent heat flux, and sensible heat flux. During both the fast response (Fig. 5e) and the slow response (Fig. 5f), it is found that while both the shortwave radiation and the latent heat flux are to release heat to the atmosphere, the longwave radiation acts to warm the ocean and the contribution from the sensible heat flux is negligible. Moreover, it can be seen that over the CEP the transition from a warming (for the fast pattern) to a cooling effect (for the slow pattern) of the surface heat flux is mainly due to the local cloud amount, which appears to increase significantly and thus leads a reduction of shortwave flux into the ocean. As this cloud radiative effect acts against the SST transition toward a more El Niño–like pattern, it should not be the cause for the transition.

Among the four components in the surface heat flux, the latent heat flux appears to be dominant over both the WEP and CEP and, as shown in Figs. 5e and 5f, exerts an important cooling effect for SST in both the fast and slow patterns. Following Du and Xie (2008), Xie et al. (2010), and Jia and Wu (2013), the latent heat flux (Q_E) can be further decomposed into the following four major terms:

$$Q'_E = \frac{\partial Q_E}{\partial T}T' + \frac{\partial Q_E}{\partial W}W' + \frac{\partial Q_E}{\partial \mathrm{RH}}\mathrm{RH}' + \frac{\partial Q_E}{\partial \Delta T}\Delta T', \qquad (6)$$

where the primes denote the differences between HEAT and CTRL. These terms on the right-hand side will be denoted as Q_{EO}, Q_{EW}, Q_{ERH}, and $Q_{E\Delta T}$, representing Newtonian cooling (Xie et al. 2010), wind–evaporation–SST (WES) feedback (Xie and Philander 1994), and contributions from change in relative humidity and air–sea surface temperature difference, respectively. As shown in Figs. 5g and 5h, for both fast and slow patterns and over both WEP and CEP, the cooling in the latent heat flux is dominated by the Newtonian cooling, while the changes in wind speed and relative humidity act to alleviate the cooling (i.e., a warming effect) and the contribution from the change in the air–sea surface temperature is negligible. In addition, with the pattern transition from the fast to the slow, Q_{EW} decreases over the WEP but increases over the CEP. This corresponds to the time evolution of wind speed in the two regions, that is, the weakening of the trade wind spreads eastward along the equatorial Pacific with time in such a way so that the WES effect increases over the CEP at the cost of WEP (cf. Figs. 4a and 4b).

Given the large internal variability of the equatorial Pacific SST and the related dynamical processes, one naturally asks whether the difference in the heat budget terms between the WEP and CEP are statistically significantly different. Two-standard deviation error bars are added to the SST and budget terms in Fig. 5 to indicate the rule-of-thumb 95% confidence intervals. Except for the fact that the SST warming itself is significantly different from zero, one can see hardly any difference between the budget for WEP versus that for CEP. Comparing between the fast and slow responses, some of the terms such as the zonal advection (UTX) indeed show distinct contribution to the budget. Taken together, caution is advised in the interpretation of the heat budget results and the related discussion above can only be taken qualitatively. To have more confidence in the coupled results, it is necessary to run many more members with the coupled model, a task beyond the affordability of our computation resource. The limited statistical confidence in the budget analysis prompts us to conduct further ocean-alone tracer experiments (where noise level is very much reduced) in section 5b.

5. Mechanisms of the pattern transition

Our modeling results suggest that the conventional ODT mechanism is dominant only during the first decade or so, and then other oceanic processes win out gradually and mask this ODT mechanism, leading to the El Niño–like condition in the quasi-equilibrated state. In this section we discuss the driving mechanisms for this transition from the fast pattern to the slow pattern.

First of all, there is little doubt that the change of the equatorial Pacific wind stress should play a role in the SST pattern transition. One of the most robust signatures of the atmospheric response to global warming is a slowdown of the Walker circulation (e.g., Vecchi and Soden 2007), which is driven by the slower rate of increase of global precipitation relative to the increase in lower-tropospheric water vapor (Held and Soden 2006). While the slower Walker circulation does induce a reduction of the zonal SST gradient along the equator, our previous overriding experiments (Luo et al. 2015) suggest that it only contributes 20% to the El Niño–like warming pattern, with the rest (80%) coming from the ocean dynamics and/or thermal coupling. Next we will show that the ocean dynamics seems to play the instigating role for the slow El Niño–like warming, especially the ocean circulation change as indicated by the passive tracer experiments.

a. Thermocline temperature adjustment

The equatorial thermocline temperature can be adjusted through its connection with the extratropics by two processes. The mean advection process (Gu and Philander 1997) suggests that extratropical SST anomalies are first subducted into the thermocline, then advected to the equator within the subsurface branch of the STC (McCreary and Lu 1994), and finally upwelled to the surface in the CEP. In contrast, the perturbation advection process (Kleeman et al. 1999) suggests that a change in the STC strength itself will alter the amount of cold extratropical thermocline water that eventually upwells in the CEP. We will demonstrate below that both processes are at work in the pattern transition in the HEAT experiments.

Figure 6 shows the warming for three epochs. During the first decade, in addition to the stronger surface warming in the WEP than in the CEP (Figs. 6a,g,j), there appear warmer waters in the eastern subtropics in both hemispheres (Fig. 6a). By the mean advection process, the eastern subtropical warmer waters from both hemispheres can subduct and penetrate through the thermocline to reach the equator and then upwell and influence the surface temperature over the CEP (Figs. 6e,f,h,i). Note that the influence from the South Pacific appears to be more direct than that from the North Pacific due to a potential vorticity island present in the north that is created by the intertropical convergence zone (Luo et al. 2005). It takes about a decade to complete this entire route, but as warming in the eastern subtropics proceeds (Figs. 6b,c), warm anomalies are growing along the pathways, contributing to the development of an El Niño–like warming pattern in the equatorial Pacific. In addition, it can be seen that the warming penetrates into deeper ocean at the equator after 30 years of the model integration (Figs. 6k,l). The time evolution of temperature in our HEAT simulations shows a considerable resemblance to Cai and Whetton (2000), who employed the CSIRO climate model to simulate the historical and project the future Pacific SST with increased GHG and found a warming pattern that has a warming initially concentrated in the western equatorial Pacific, but moving to the eastern Pacific eventually.

On the other hand, the STC itself is found to slow down with the time evolution. As elucidated in Fig. 7, the STC transport is reduced by about 1.5 Sv (1 Sv $\equiv$ $10^6\,m^3\,s^{-1}$) from 57.0 to 55.5 Sv during the first decade, and then the reduction continues at a slower pace until reaching ~54.0 Sv at year 50. Since the STC transports warmer water out of the tropics within the surface layer and brings colder water in the thermocline from the subtropics back to the equator, its reduction in strength implies a net warming in the CEP region and hence the development of the El Niño–like warming pattern. It should be added that the slowdown of the STC could originate from either the change of wind stress along the equator or a pure oceanic adjustment to warming, or both. However, the coupled HEAT experiments are incapable of distinguishing these two sources. Therefore, we have to resort to experiments with the ocean model to unambiguously identify an oceanic origin for the El Niño–like warming.

b. Passive tracer experiments

To further diagnose the origin of the initial minimum warming and the slow transition to the El Niño–like warming in the eastern equatorial Pacific, we employ a passive tracer to POP2 ocean model in order to isolate the contribution to the SST change due to the passive advection by the background mean ocean current from that due to the change of ocean circulation. The response in the SST perturbation run (T'), P_1' tracer run, P_2' tracer run, and the difference of $T' - P_2'$ are presented in Fig. 8. Interestingly, both T' and the two passive tracers show a warming minimum in the eastern equatorial Pacific and hence a La Niña–like pattern during the first decade, suggesting strongly an oceanic origin of the initial lack of warming in the eastern equatorial Pacific. Meanwhile, the redistributive temperature change (T_r') compensates the spatial structure of the passive tracers toward an El Niño–like condition during the first decade. In our experiment configuration, T_r' is the result of both ocean circulation change and modification on the surface heat uptake through the ocean temperature redistribution. The latter, inferred from the difference between Q' and Q_p', turns out to be cooling the eastern

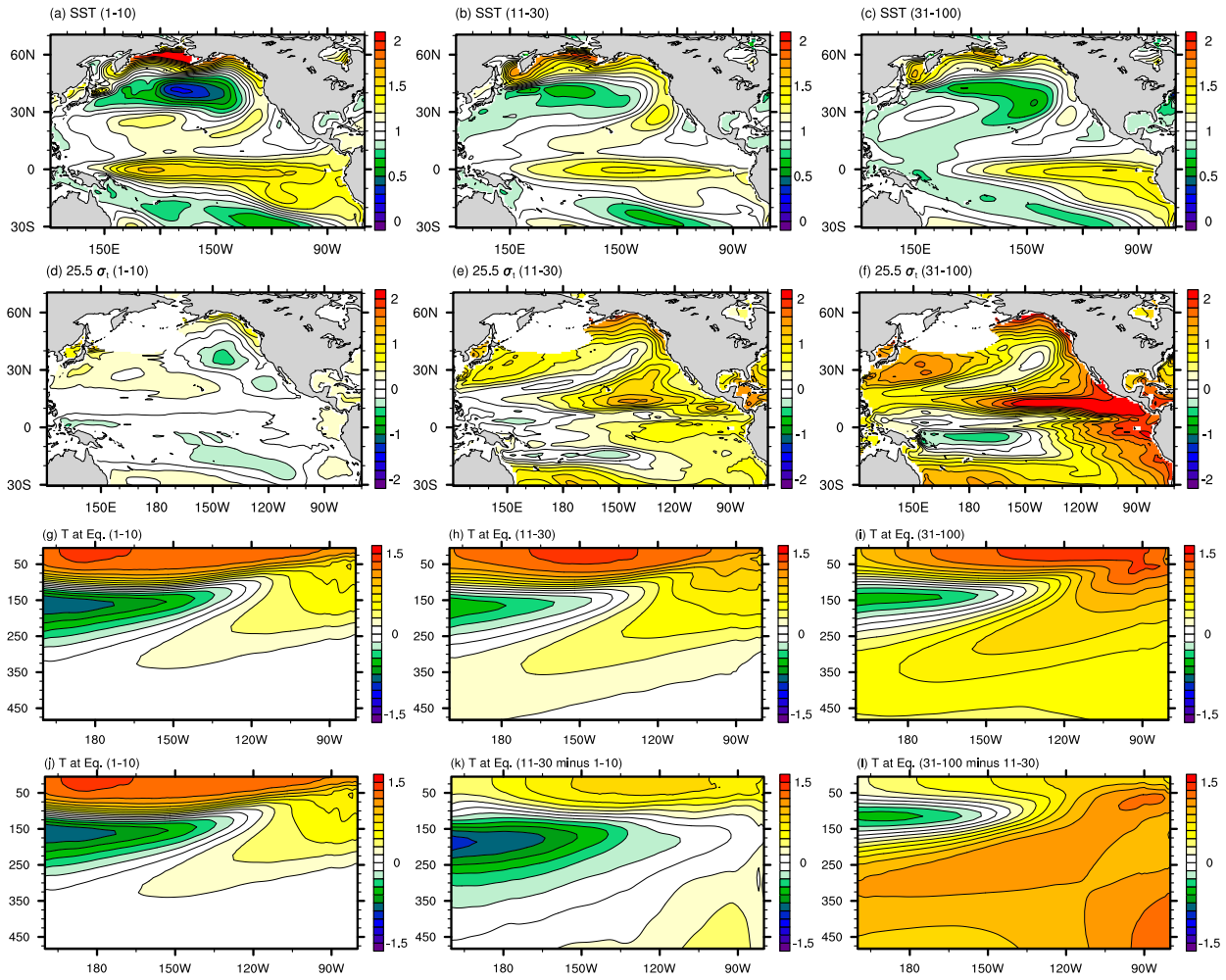

FIG. 6. The uniform heating induced temperature changes during three periods of years: (left) 1–10, (center) 11–30, and (right) 31–100. Shown are the (a)–(c) SST warming over the Pacific Ocean, (d)–(f) warming along the 25.5 kg m^{-3} isopycnal surface, (g)–(i) warming at the equator, and (j)–(l) propagation of the warming along the equator. The SST warming in (a)–(c) has been normalized by global-mean SST change during the corresponding time period.

Pacific during the early stage of the response. Therefore, the warming effect in T'_r is totally dynamically induced, possibly due to the weakening of the Pacific subtropical overturning cell in the perturbation run (but it should not be confused with the wind-driven part of the weakening, since this is an ocean-alone experiment). The weakening of the STC is further confirmed by the time series of the maximum meridional overturning streamfunction in the Pacific (not shown). This redistributive warming effect is overwhelmed by the anomalous ocean dynamical cooling effect revealed by the passive tracers, and hence a La Niña–like initial response in T' results. The patterns of the surface heat fluxes seem to reflect the difference between the model SST or P' and the target temperature anomaly, with a greater difference leading to a greater heat flux into the ocean (Fig. 9).

The slow transition to a warmer SST condition in the eastern Pacific from year 11 to 50 (Fig. 8, left column) seems to originate from the passive advection and diffusion by the mean ocean circulation as well. It is especially worth noting that T' transitions from an anomalous cooling in the eastern Pacific during the first decade to a warming in the fifth decade despite the cooling from the surface flux, thus pointing to an ocean dynamical origin of the slow SST warming trend. Indeed, turning to the tracer evolution, this gradual warming trend results largely from the gradual decay of the feature of the anomalous cooling in P'_2 patterns, which are purely induced by the passive advection by the background mean circulation in the picontrol run. In view of the gradual decay of the cooling in the P'_2 pattern and the weakening trend of the STC in the

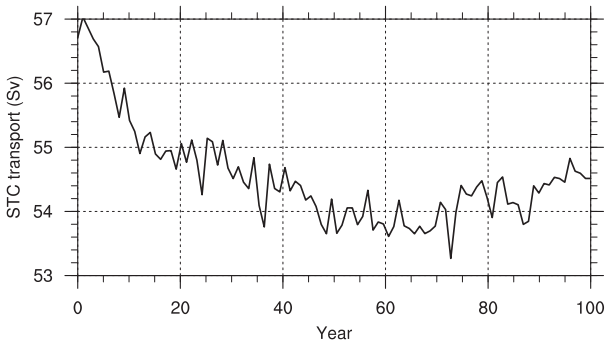

FIG. 7. Time series of the maximum meridional overturning streamfunction for the Pacific (i.e., the Pacific STC transport) in the coupled simulations with CESM1.1.

corresponding experiment, one might speculate that the slow transition to relatively less cold condition in the eastern Pacific arises from the weakening of the STC. However, the P_1' tracer experiment based on the perturbation ocean condition exhibits almost identical evolution to that of the P_2' tracer (cf. the middle two columns of Fig. 8), ruling out the importance of the advective effect on the passive tracer by the anomalous part of the ocean circulation (although this effect is still discernable). As a result, the slow decaying trend in the cooling in the eastern Pacific (middle two panels in Fig. 8) can be only attributed to the arrival of warm water from the subsurface pathways (i.e., the thermocline).

One might be attempted to attribute the weakening trend of the P_1' and P_2' patterns to the surface flux, which is always directed into the ocean in the eastern Pacific. However, by our experimental design the tracer is restored to a constant surface anomaly at a constant relaxation time scale, so the oceanic uptake of the tracer should have been uniform in space were it not for the heterogeneity in the dynamically induced tracer convergence/divergence by the mean ocean circulation. The slower warming in the tracer field indicates a longer time scale for the tracer to adjust toward the target value due to the modulation on the response time scale by the local ocean dynamical processes. Therefore, the spatial patterns in the surface heat uptake of P_1' and P_2' (representative of heat flux) shown in the middle two columns in Fig. 9 are the passive manifestations of the ocean dynamical thermostat on the surface flux, but not the active surface driving for the pattern evolution of the passive tracers. Given the essential role of the passive tracers on the T' evolution, the same notion can be applied for T' as well.

During that period, the redistributive SST anomalies $(T' - P_2')$ feature a slight weakening trend in its El Niño–like pattern (Fig. 8, right column), thus not contributing to the slow transition to the El Niño state. This result lends further support to the role of the thermocline adjustment in the slow SST warming over the eastern equatorial Pacific discussed in the previous subsection.

6. Summary and discussion

The conventional ODT refers to the cooling effect from the ocean in the eastern equatorial Pacific by a vertical advection against the sharp and shallow thermocline thus ventilating the mixed layer with cold water from below. This ODT can potentially give rise to a La Niña–like SST pattern upon a uniform surface warming for the ocean. However, a majority of climate models projects an El Niño–like SST response in the equatorial Pacific to global warming. This implies that the conventional ODT is masked by other processes that contribute positively to the eastern Pacific SST warming. Here, inspired by the earlier ODT studies, we have performed ODT-type experiments using both a fully coupled atmosphere–ocean GCM and its ocean component to examine how the conventional ODT and the extension thereof work to initiate a fast west-centered SST warming and a slow El Niño–like warming in the equatorial Pacific. This SST evolution in the coupled ODT experiments exhibits considerable resemblance to that of the coupled response forced by an abrupt increase of GHGs. The fast and slow responses of the evolution are illustrated schematically in Figs. 10a and 10b, respectively. The transition from the fast pattern to the slow pattern is accompanied by a weakening of the equatorial easterlies and an increase of thermocline temperature at the equator, with the latter playing a more important role. The weakened equatorial easterlies are associated with a slowdown of the Walker circulation, which is a robust signature of the atmospheric response to global warming. The increased equatorial thermocline temperature is attributable to both the warm extratropical waters advected to the equator within the subsurface branch of the STC and a reduction of the STC strength itself.

Our experiments show that the fast response characteristic of lack of warming in the CEP to the uniform surface heat flux indeed originates from the conventional ODT mechanism (i.e., the cold advection by background upwelling). On the other hand, the slowly evolving El Niño–like SST warming (slow pattern) comes about from two ocean dynamical sources: 1) the weakening of the STC due to both the weakened trade wind and the dynamical adjustment to the enhanced ocean stratification by the surface uniform heat flux and

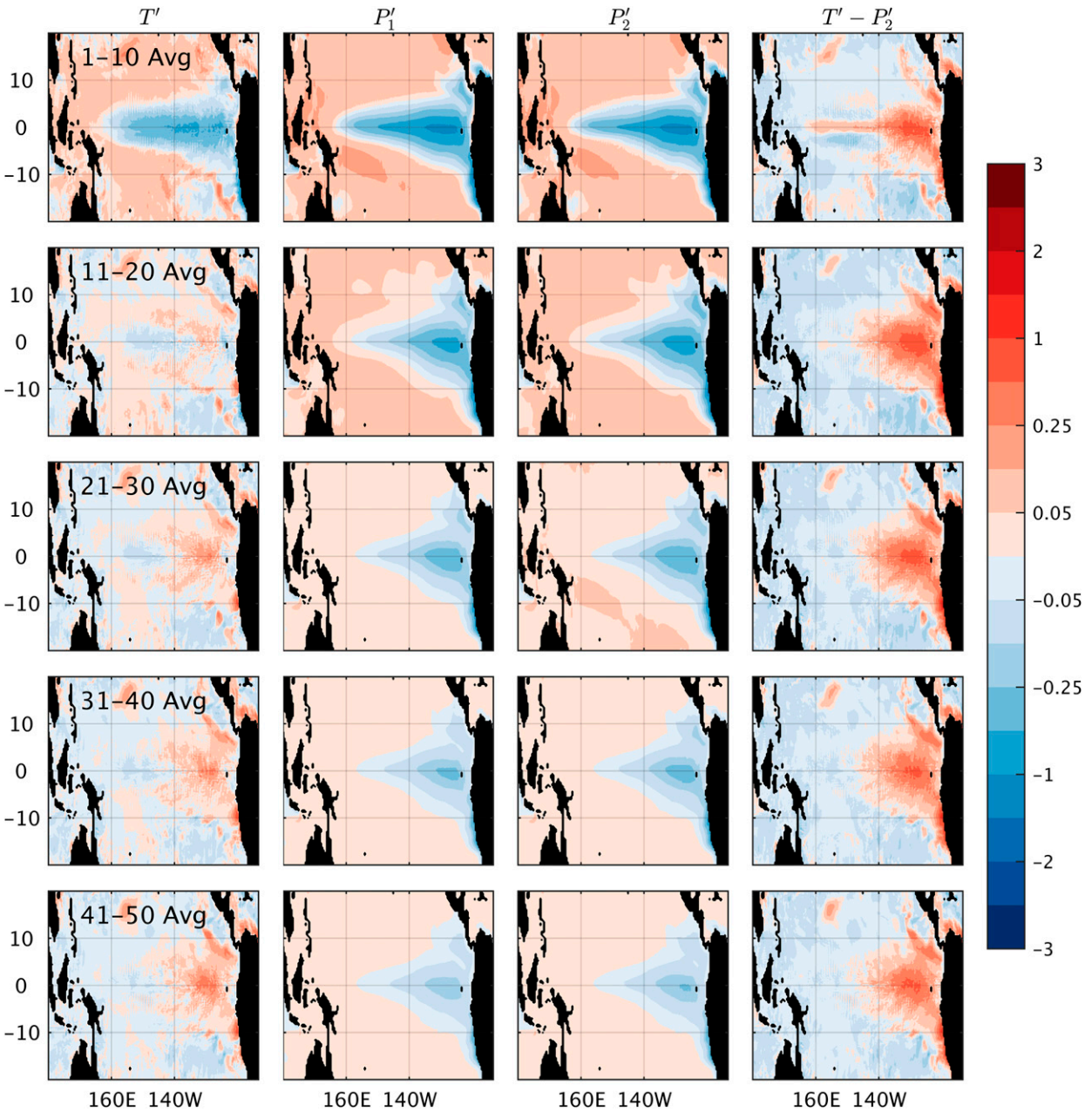

FIG. 8. Time evolution of SST anomalies associated with, from left to right, T', passive tracer P_1', passive tracer P_2', and inferred redistributive SST pattern $T_r' = T' - P_2'$ from the tracer experiments with POP2. In each panel, the mean over the tropical Pacific is removed to highlight the spatial pattern of the evolution.

2) the slow arrival of the relatively warmer subtropical water to the equatorial mixed layer via the thermocline. It is only through a set of passive tracer experiments with the ocean component of CESM1.1 that one can pinpoint the latter process. This might also be the process that sets the pace of the slow adjustment—the time it takes for the subtropical water to arrive at the eastern equatorial Pacific. Why an intensification of upper ocean stratification should lead to a weakening of the STC remains an open question for future investigation.

Our ODT experiments and their mixed layer heat budget analysis work to generalize the meaning of the ODT. If ODT is to encapsulate the full ocean dynamical effect (thus including the horizontal advection and mixing) upon a uniform flux perturbation, it can exert complex impacts with an initial anomalously cooling and

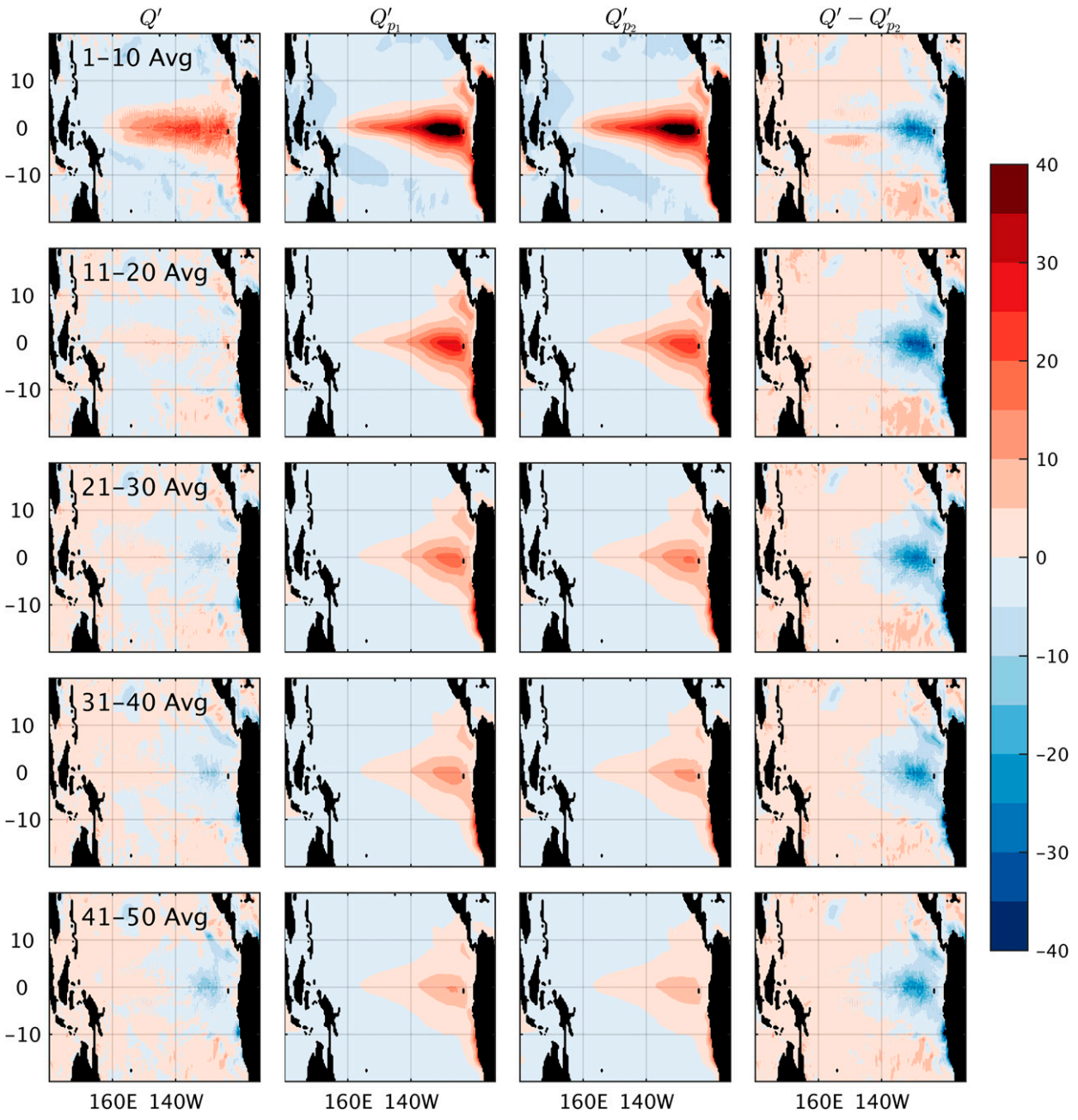

FIG. 9. As in Fig. 8, but for surface heat flux.

later warming on the mixed layer water in the eastern equatorial Pacific, whereas the conventional ODT works only to cool the mixed layer. Allowing this generalized ODT to feed back to the atmosphere (and hence to extend the ODT further to a coupled system), as in the coupled ODT experiments, may conceivably draw the westerly wind anomalies eastward. If this were the case, the *slow* evolution of the tropical wind response in the coupled ODT experiments would also be traceable to an ocean dynamical origin. Further passive tracer experiments with coupled atmosphere–ocean GCM will be needed to confirm this hypothesis.

The ODT experiments by design have down played the effect of the atmospheric feedbacks with the ocean-alone tracer experiments eliminating these feedbacks all together. Previous studies have proposed that the negative SST–convective feedback over the western Pacific warm pool is responsible for the El Niño–like warming

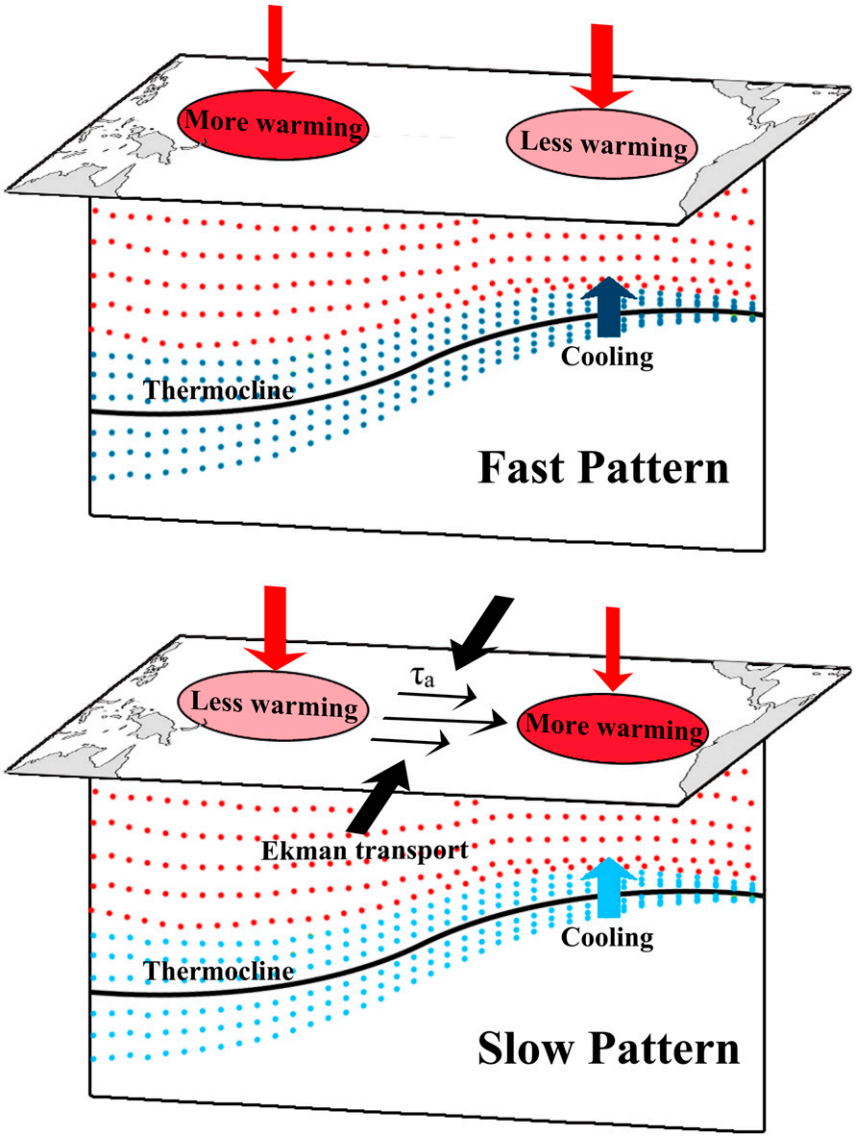

FIG. 10. Schematics depicting the changes in the equatorial Pacific for the (top) fast and (bottom) slow response patterns. The red arrows indicate the heat fluxes into the ocean, with big arrows for more heat and small arrows for less heat. The red dots represent the warm mixed layer water. The dark (upper) and light (lower) blue dots represent the cold thermocline waters, with the latter being relatively warmer than the former; correspondingly, the dark (upper) and light (lower) blue arrows denote the vertical cooling in the two situations, respectively. The thermocline depths are represented by thick black lines. In the lower panel, small black arrows indicate anomalous zonal wind stress, which induces less divergence of surface warm water via Ekman transport that is indicated by big black arrows.

pattern (Meehl and Washington 1996; Li et al. 2016). As this atmospheric feedback operates at a much faster time scale, it should not set the pace of the slow transition to the El Niño–like condition. Moreover, the surface energy budget carried out here shows that the slow transition is accompanied by a cloud radiative cooling extending to the central and eastern Pacific. Thus, it is unlikely that the SST–convective feedback plays a positive role in the slow SST pattern transition. On the other hand, although the analysis of the coupled model results cannot rule out the possibility that the fast La Niña–like response pattern might arise from the underestimation of the negative SST–convective feedback over the warm pool region that is a common bias shared by many climate models (Li and Xie 2012, 2014; Li et al. 2015), our ocean-alone tracer experiments excluding

this feedback still produce a strong La Niña–like warming pattern during the first decade, underlining the importance of ocean dynamics for this pattern formation.

Acknowledgments. We thank two anonymous reviewers for their helpful comments and suggestions that have enabled us to significantly improve the article. This work is supported by the National Natural Science Foundation of China (NSFC; 41376009 and 41676002) and the National Science Foundation (NSF; AGS-1249173 and AGS-1249145). Y. Luo would also like to acknowledge the support from the Zhufeng and Taishan Projects of the Ocean University of China. J. Lu is supported by the Office of Science of the U.S. Department of Energy as part of its Regional and Global Climate Modeling program.

REFERENCES

Andrews, T., J. M. Gregory, and M. J. Webb, 2015: The dependence of radiative forcing and feedback on evolving patterns of surface temperature change in climate models. *J. Climate*, **28**, 1630–1648, doi:10.1175/JCLI-D-14-00545.1.

Banks, H. T., and J. M. Gregory, 2006: Mechanisms of ocean heat uptake in a coupled climate model and the implications for tracer based predictions of ocean heat uptake. *Geophys. Res. Lett.*, **33**, L07608, doi:10.1029/2005GL025352.

Cai, W., and P. H. Whetton, 2000: Evidence for a time-varying pattern of greenhouse warming in the Pacific Ocean. *Geophys. Res. Lett.*, **27**, 2577–2580, doi:10.1029/1999GL011253.

Clement, A. C., R. Seager, M. A. Cane, and S. E. Zebiak, 1996: An ocean dynamical thermostat. *J. Climate*, **9**, 2190–2196, doi:10.1175/1520-0442(1996)009<2190:AODT>2.0.CO;2.

DiNezio, P. N., A. C. Clement, G. A. Vecchi, B. J. Soden, B. P. Kirtman, and S.-K. Lee, 2009: Climate response of the equatorial Pacific to global warming. *J. Climate*, **22**, 4873–4892, doi:10.1175/2009JCLI2982.1.

——, ——, and ——, 2010: Reconciling differing views of tropical Pacific climate change. *Eos, Trans. Amer. Geophys. Union*, **91**, 141–142, doi:10.1029/2010EO160001.

Du, Y., and S.-P. Xie, 2008: Role of atmospheric adjustments in the tropical Indian Ocean warming during the 20th century in climate models. *Geophys. Res. Lett.*, **35**, L08712, doi:10.1029/2008GL033631.

Garuba, O. A., and B. Klinger, 2016: Ocean heat uptake and interbasin transport of the passive and redistributive components of surface heating. *J. Climate*, **29**, 7507–7527, doi:10.1175/JCLI-D-16-0138.1.

Gregory, J. M., 2000: Vertical heat transports in the ocean and their effect on time-dependent climate change. *Climate Dyn.*, **16**, 501–515, doi:10.1007/s003820000059.

Gu, D., and S. G. H. Philander, 1997: Interdecadal climate fluctuations that depend on exchanges between the tropics and extratropics. *Science*, **275**, 805–807, doi:10.1126/science.275.5301.805.

Held, I. M., and B. J. Soden, 2006: Robust responses of the hydrological cycle to global warming. *J. Climate*, **19**, 5686–5699, doi:10.1175/JCLI3990.1.

——, M. Winton, K. Takahashi, T. Delworth, F. Zeng, and G. K. Vallis, 2010: Probing the fast and slow components of global warming by returning abruptly to preindustrial forcing. *J. Climate*, **23**, 2418–2427, doi:10.1175/2009JCLI3466.1.

Jia, F., and L. Wu, 2013: A study of response of the equatorial Pacific SST to doubled-CO_2 forcing in the coupled CAM–1.5-layer reduced-gravity ocean model. *J. Phys. Oceanogr.*, **43**, 1288–1300, doi:10.1175/JPO-D-12-0144.1.

Kleeman, R., J. P. McCreary Jr., and B. A. Klinger, 1999: A mechanism for generating ENSO decadal variability. *Geophys. Res. Lett.*, **26**, 1743–1746, doi:10.1029/1999GL900352.

Knutson, T. R., and S. Manabe, 1995: Time-mean response over the tropical Pacific to increased CO_2 in a coupled ocean–atmosphere model. *J. Climate*, **8**, 2181–2199, doi:10.1175/1520-0442(1995)008<2181:TMROTT>2.0.CO;2.

Knutti, R., S. Krähenmann, D. J. Frame, and M. R. Allen, 2008: Comment on ''Heat capacity, time constant, and sensitivity of Earth's climate system'' by S. E. Schwartz. *J. Geophys. Res.*, **113**, D15103, doi:10.1029/2007JD009473.

Li, C., J.-S. von Storch, and J. Marotzke, 2013: Deep-ocean heat uptake and equilibrium climate response. *Climate Dyn.*, **40**, 1071–1086, doi:10.1007/s00382-012-1350-z.

Li, G., and S.-P. Xie, 2012: Origins of tropical-wide SST biases in CMIP multi-model ensembles. *Geophys. Res. Lett.*, **39**, L22703, doi:10.1029/2012GL053777.

——, and ——, 2014: Tropical biases in CMIP5 multimodel ensemble: The excessive equatorial Pacific cold tongue and double ITCZ problems. *J. Climate*, **27**, 1765–1780, doi:10.1175/JCLI-D-13-00337.1.

——, Y. Du, H. Xu, and B. Ren, 2015: An intermodel approach to identify the source of excessive equatorial Pacific cold tongue in CMIP5 models and uncertainty in observational datasets. *J. Climate*, **28**, 7630–7640, doi:10.1175/JCLI-D-15-0168.1.

——, S.-P. Xie, Y. Du, and Y. Luo, 2016: Effects of excessive equatorial cold tongue bias on the projections of tropical Pacific climate change. Part I: The warming pattern in CMIP5 multi-model ensemble. *Climate Dyn.*, **47**, 3817–3831, doi:10.1007/s00382-016-3043-5.

Liu, F., Y. Luo, J. Lu, and X. Wan, 2016: Response of the tropical Pacific Ocean to El Niño versus global warming. *Climate Dyn.*, doi:10.1007/s00382-016-3119-2, in press.

Long, S.-M., S.-P. Xie, X.-T. Zheng, and Q. Liu, 2014: Fast and slow responses to global warming: Sea surface temperature and precipitation patterns. *J. Climate*, **27**, 285–299, doi:10.1175/JCLI-D-13-00297.1.

Luo, Y., L. M. Rothstein, R.-H. Zhang, and A. J. Busalacchi, 2005: On the connection between South Pacific subtropical spiciness anomalies and decadal equatorial variability in an ocean general circulation model. *J. Geophys. Res.*, **110**, C10002, doi:10.1029/2004JC002655.

——, J. Lu, F. Liu, and W. Liu, 2015: Understanding the El Niño-like oceanic response in the tropical Pacific to global warming. *Climate Dyn.*, **45**, 1945–1964, doi:10.1007/s00382-014-2448-2.

McCreary, J. P., Jr., and P. Lu, 1994: Interaction between the subtropical and equatorial ocean circulations: The subtropical cell. *J. Phys. Oceanogr.*, **24**, 466–497, doi:10.1175/1520-0485(1994)024<0466:IBTSAE>2.0.CO;2.

Meehl, G. A., and W. M. Washington, 1996: El Niño-like climate change in a model with increased atmospheric CO_2 concentrations. *Nature*, **382**, 56–60, doi:10.1038/382056a0.

Seager, R., and R. Murtugudde, 1997: Ocean dynamics, thermocline adjustment, and regulation of tropical SST. *J. Climate*, **10**, 521–534, doi:10.1175/1520-0442(1997)010<0521:ODTAAR>2.0.CO;2.

——, M. B. Blumenthal, and Y. Kushnir, 1995: An advective atmospheric mixed layer model for ocean modeling purposes: Global simulation of surface heat fluxes. *J. Climate*, **8**, 1951–1964, doi:10.1175/1520-0442(1995)008<1951:AAAMLM>2.0.CO;2.

Vecchi, G. A., and B. J. Soden, 2007: Global warming and the weakening of the tropical circulation. *J. Climate*, **20**, 4316–4340, doi:10.1175/JCLI4258.1.

——, A. C. Clement, and B. J. Soden, 2008: Examining the tropical Pacific's response to global warming. *Eos, Trans. Amer. Geophys. Union*, **89**, 81–83, doi:10.1029/2008EO090002.

Xie, P., and G. K. Vallis, 2012: The passive and active nature of ocean heat uptake in idealized climate change experiments. *Climate Dyn.*, **38**, 667–684, doi:10.1007/s00382-011-1063-8.

Xie, S.-P., and S. G. H. Philander, 1994: A coupled ocean-atmosphere model of relevance to the ITCZ in the eastern Pacific. *Tellus*, **46A**, 340–350, doi:10.1034/j.1600-0870.1994.t01-1-00001.x.

——, C. Deser, G. A. Vecchi, J. Ma, H. Teng, and A. T. Wittenberg, 2010: Global warming pattern formation: Sea surface temperature and rainfall. *J. Climate*, **23**, 966–986, doi:10.1175/2009JCLI3329.1.